Quasi-thresholdless Photon Upconversion in Metal-Organic Framework Nanocrystals

F. Meinardi[1], M. Ballabio[1], N. Yanai[2], N. Kimizuka[2], A. Bianchi[1], M. Mauri[1], R. Simonutti[1], A. Ronchi[1], M. Campione[3] and A. Monguzzi[1]*

[1]Dipartimento di Scienza dei Materiali, Università Milano Bicocca,
via R. Cozzi 53, 20125 Milano - ITALY

[2]Department of Chemistry and Biochemistry, Graduate School of Engineering, Center for Molecular Systems (CMS), Kyushu University, Moto-oka 744, Nishi-ku, Fukuoka-819-0395, Japan

[3]Department of Earth and Environmental Sciences, Università degli Studi Milano-Bicocca, Piazza della Scienza 4, 20126 Milano, Italy

Keywords: photon upconversion - triplet-triplet annihilation - nanocomposite – nanocrystals – metal organic frameworks

Abstract.
Photon upconversion based on sensitized triplet-triplet annihilation (*s*TTA) is considered a promising strategy for the development of light-managing materials aimed to enhance the performance of solar devices by recovering unused low energy photons. Here, we demonstrate that, thanks to the fast diffusion of excitons, the creation of triplets pairs in metal-organic framework nanocrystals (*n*MOFs) with size smaller than the exciton diffusion length implies a 100% TTA yield regardless the illumination condition. This makes each *n*MOFs a thresholdless, single-unit annihilator. We develop a kinetic model for describing the upconversion dynamics in a nanocrystals ensemble, which allows defining the threshold excitation intensity I_{th}^{box} required to reach the maximum conversion yield. For materials based on thresholdless annihilators, I_{th}^{box} is determined by the statistical distribution of the excitation energy among nanocrystals. The model is validated by fabricating a nanocomposite material based on *n*MOFs, which shows efficient upconversion under few percent of solar irradiance matching the requirements of real life solar technologies. The statistical analysis reproduces the experimental findings, and represents a general tool for predicting the optimal compromise between dimensions and concentration of *n*MOFs with a given crystalline structure that minimize the irradiance at which the system starts to be fully operating.

In the last decade, the research on phenomena that involve the triplet state in organic systems, such as singlet-fission (SF)[1, 2] and thermally activated delayed fluorescence (TADF),[3, 4] received increased attention due to their potential application to solar cells and organic light emitting diodes technologies. Another important mechanism involving triplet states is the photon upconversion based on sensitized triplet-triplet annihilation (*s*TTA), which is considered a promising strategy for the development of light-managing materials aimed at enhancing the performance of solar devices by recovering unused low energy photons.[5-10] As sketched in Fig. 1a, the *s*TTA upconversion relies on the annihilation of two optically dark triplets (TTA) of an emitter moiety, with energy below the device bandgap, which produces a high energy fluorescent singlet that emits a photon suitable to be absorbed.[11-15] Dark triplets are sensitized through triplet-triplet Dexter energy transfer (ET) from a light-harvester, which implies that the *s*TTA upconversion is obtained in bi-component systems such as mixtures of the light-harvester/sensitizer and the annihilator/emitter moieties. Remarkably, in composition-optimized systems upconversion quantum efficiencies (QY_{uc}) larger than 30% can be achieved with excitation light intensities comparable to the solar irradiance, paving the way for real world applications of this photon managing technique.[16]

It is worth pointing out that excited molecules in solution or molecular excitons in solids should collide in order to experience ET and TTA, because both of them occur *via* a short-range electron exchange mechanism.[17, 18] The triplets diffusion dynamic is therefore crucial to obtain high performance upconverting materials and devices.[19, 20] In particular, because of the bimolecular nature of TTA, the QY_{uc} is not a constant as like for standard photoluminescence, but it depends on the excitation intensity I_{exc}. By setting the number of available excitons, it determines both the annihilation rate (k_{TTA}) and yield (ϕ_{TTA}), i.e. the fraction of triplet deactivated by annihilation.[21] It is easy to observe experimentally that at low intensities, when k_{TTA} is negligible, the upconversion efficiency depends linearly on I_{exc}. Conversely, at high

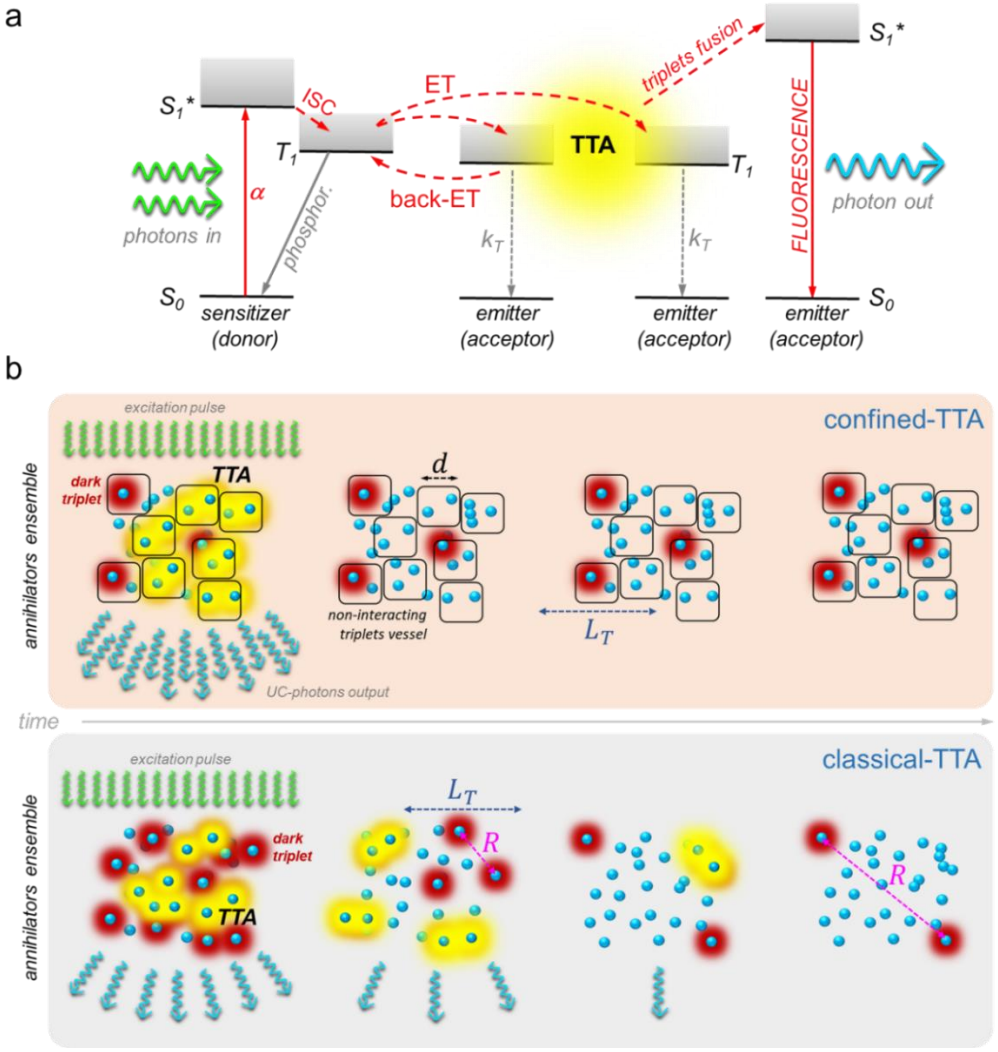

Figure 1. a) A sensitizer with absorption coefficient α is excited into a singlet state (S_1*) that efficiently undergoes intersystem crossing (ISC) into the triplet state (T_1). Energy transfer (ET) then competes with back energy transfer (back-ET) to emitter triplets. These triplets can either spontaneously decay (with rate constant k_E) or undergo triplet−triplet annihilation (TTA) to an excited fluorescent singlet state of the emitter. Dashed lines mark a radiation-less transition. b) Sketch of the TTA mechanism upon pulsed excitation in a confined system, where triplets pairs are collected in non-interacting vessels of size d shorter than their diffusion length L_T forcing their annihilation (top panel), and in a classical bulk material, where the average distance between triplets pairs R change with time (low panel).

irradiances when the TTA becomes dominant, the ϕ_{TTA} approaches 100% and QY_{uc} saturates to its maximum value QY_{uc}^{max}, being limited only by the statistical probability f to form a singlet upon triplets annihilation, by the ET efficiency ϕ_{ET}, and by the emitter fluorescence yield QY_{fl}.[21-23] For solar applications, it is therefore mandatory that the irradiance required for QY_{uc}^{max}, the so-called excitation intensity threshold I_{th},[21] is significantly lower than one sun to maximize the conversion efficiency regardless the illumination condition during daytime. In

order to fulfill this constraint, triplets should possess a large diffusion length L_T that ensures high collisional probability even at low irradiances when their concentration is small. In other words, a fast diffusion environment is required to have L_T larger than the average distance R between two triplets, thus allowing their encounter and annihilation before spontaneous recombination to the ground state.[24]

The fast diffusion requirement is fulfilled in metal-organic framework nanocrystals (*n*MOFs). A *n*MOF consists of an ordered network of emitter molecules interconnected by metal ions.[25] These structures preserve both the properties of the constituent fluorophores, which do not interact with each other, and the high exciton mobility of crystalline molecular aggregates.[26] The *s*TTA upconversion in *n*MOFs has been already proven but with limited efficiency because of the small QY_{fl} that characterizes these materials.[27, 28] However, we recently demonstrated that the poor emission efficiency mainly arises from the presence of surface defects that act as quenchers. A proper surface passivation enables to obtain highly emissive nanocrystals,[26] which then represent the ideal components for realizing upconverting materials based on TTA. The availability of nanosized upconverters is indeed pivotal for the realization of composite materials with tailored optical properties, which can be implemented in current technologies or that can represent new archetypes for more complex photonic systems.

The modelling of the *s*TTA upconversion in nanosized systems is therefore mandatory in order to point out the limiting factors of the material performance, and thus the guidelines for the design and synthesis of efficient upconverters at low powers. Specifically, we focus our attention on *n*MOFs with dimension d of few tenths of nanometers where the condition $L_T >> d$ is always verified for triplet excitons (confined-TTA).[29-31] It implies that each triplets pair created in a single *n*MOF annihilates before spontaneous recombination avoiding energy dissipation, thus achieving a ϕ_{TTA} = 100%. Therefore, each *n*MOF can be considered as an individual, thresholdless annihilator, under the only condition that at least two triplets are created in the same nanocrystal. Otherwise, upconversion is not allowed and isolated triplets

decay spontaneously. Notably, this peculiar annihilation dynamics can be evidenced by means of time resolved photoluminescence spectroscopy experiments. As sketched in the top panel of Fig.1b, under pulsed excitation the upconverted light is immediately generated in nanocrystals where at least two triplets are created, while no emission can be detected at longer times from *n*MOFs where a single triplet survives. This behavior is radically different from classical *s*TTA upconversion in bulk materials (classical-TTA), where an infinite volume is accessible to excitons. In this case, after the excitation pulse the intensity of the upconverted emission progressively decreases with the time until the density of triplets is reduced to the point that $L_T << R$, thus avoiding their encounter (low panel).[32, 33]

Here, we analyze the *s*TTA upconversion in a nanocomposite based on a *n*MOF dispersion in poly(*butyl*-acrylate). The sensitization of the nanocrystal triplets occurs via ET from diffusing metallated porphyrins embedded in the host matrix. The confined–TTA process is described by a kinetic model that takes into account the statistical distribution of excitons in an ensemble of nanocrystals upon steady state photo-excitation. The model predicts a new kind of threshold excitation intensity $\left(I_{th}^{box}\right)$ for thresholdless annihilators, which marks the excitation fluency required to fully activate the upconversion in the ensemble. The observed I_{th}^{box} corresponds to an irradiance of ~0.05 suns, highlighting once more the potential of *s*TTA upconversion for solar technologies. The threshold can be predicted by using few fundamental parameters characteristic of the nanocomposite measured independently, being therefore a powerful figure of merit for the design of next generation quasi-thresholdless upconverters for a large variety of photonic applications.

As sketched Fig. 2, photon upconversion is obtained in a nanocomposite made of fluorescent *n*MOFs embedded in a polyacrylate elastomeric matrix doped with sensitizers. The rubber matrix results in a bulk material suitable for applications, providing at the same time the passivation of *n*MOF surfaces required for high-performance upconversion. Each *n*MOF

behaves as a triplets collector, a sink for the energy harvested by the sensitizers that diffuse in the viscous host polymer and transfer this energy to nanocrystals upon collision. [34-36] Figure 2a illustrates the building blocks employed to fabricate *n*MOFs. The organic ligand used is the fluorescent 4,4'-(anthracene-9,10-diyl)dibenzoate (ADB). The ADB units are bound to Zn^{2+} ions thanks to the lateral phenyl rings, which are terminated with carboxylic groups thus enabling the growth of self-assembled frameworks. The employed microwave-assisted synthesis results in a white powder of nanocrystals with an average size of ~26 nm, as observed by transmission electron microscopy (TEM, Fig. 2b and Supplementary Fig. S1). The x-rays diffraction analysis (Fig. S2) indicates that the closest center-to-center distance between two ligands in *n*MOFs is ~0.9 nm, which is a distance that allows the triplets diffusion within the framework by homo-molecular Dexter energy transfer.[37, 38] The details of the *n*MOF synthesis and crystalline structure are reported in Methods section and in the Supplementary Information (SI) file. The top panel of Fig. 2c reports the photoluminescence and the photoluminescence excitation spectra of a nanocrystals dispersion in benzene. Upon UV excitation at 340 nm the *n*MOFs show a blue emission peaked at 440 nm with a fluorescence quantum yield QY_{fl} = 17%. By considering that the electronic properties of the ADB ligand are strictly similar to that of its precursor dye, namely the 9,10 *di*-phenylanthracene (DPA), we select the Pt(II)-octaetyl porphyrin (PtOEP) as light harvester, which is an effective sensitizer of DPA triplets.[39] When excited in the lowest absorption band at 532 nm (Fig. 2c, low panel), the PtOEP undergoes fast intersystem crossing populating its phosphorescent triplet state. From here, when a sensitizer molecule hits the nanocrystals surfaces, the ET occurs to the triplet of the ADB molecules incorporated in the *n*MOF.[11] Once verified the upconverting ability of *n*MOFs in benzene solution with PtOEP (Fig. S3), we fabricate the *s*TTA nanocomposite by mixing 3 mg of *n*MOFs with 1 ml of a *butyl*- acrylate/PtOEP solution (2×10^{-4} M). Free radical polymerization of *butyl*- acrylate leads to the formation of *polybutyl*-acrylate, a rubbery polymer with glass transition temperature of about 220 K. In this case, the polymerization is conducted at room

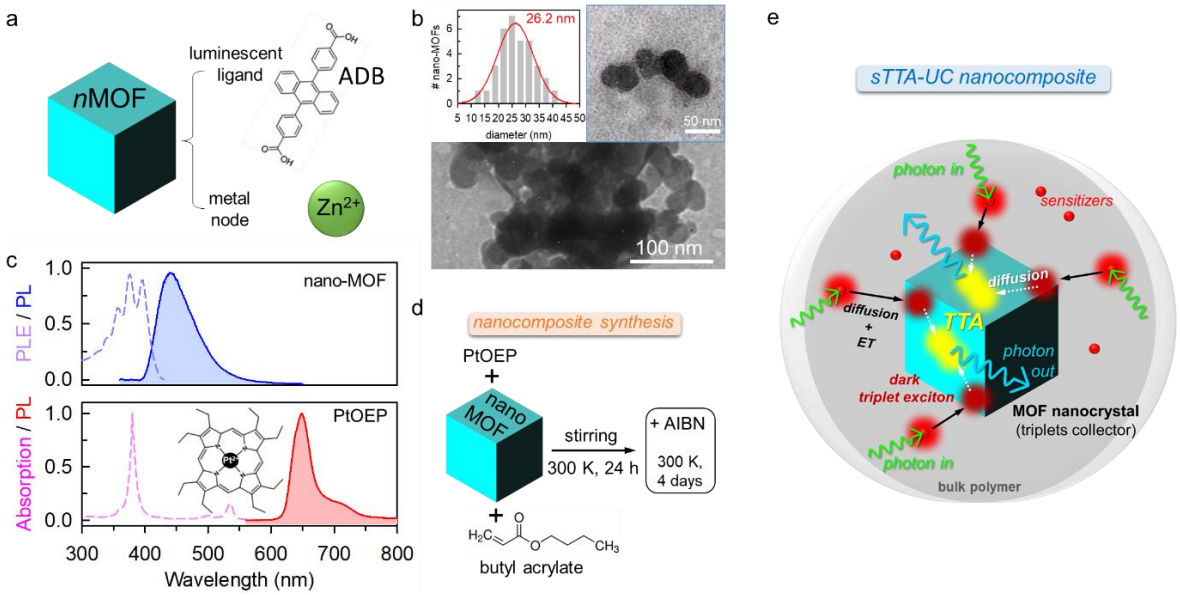

Figure 2. a) Sketch of the *n*MOF composition and b) transmission electron microscopy (TEM) image of drop casted bare *n*MOFs. The inset shows the nanocrystals size distribution. c) Photoluminescence (PL), photoluminescence excitation (PLE) and absorption spectra of *n*MOFs and sensitizers PtOEP in benzene dispersion. The PtOEP molecular structure is reported as inset. d) Scheme of the synthesis route followed for the fabrication of the nanocomposite. e) Schematics of the *s*TTA upconversion mechanism in the material. Upon absorption of green photons, sensitizers diffuse in the polymer and subsequently transfer the absorbed energy by ET upon collision with the embedded MOF nanocrystals (*n*MOFs), which acts as triplet exciton collectors. Dark triplet excitons on the *n*MOF organic ligands, generated on the surfaces, diffuse within the crystal and undergoes TTA producing fluorescent blue emitting singlets.

temperature for days (Fig. 2d) by the addition of the radical polymerization initiator 2,2'azobis(isobutyronitrile) (AIBN, 0.1 mg). AIBN is one of the most used free radical initiators, it is thermally activated with a rate constant k_d of 2.15×10^{-7} (s^{-1}) at 313 K in CCl_4.[40] Therefore, by performing the polymerization at room temperature the number of free radicals generated should be sufficiently low to ensure very high molecular weights, because furthermore combination and disproportionation reactions should be negligible. The material is prepared and sealed in a glove box under controlled nitrogen atmosphere. The selection of the poly *butyl*-acrylate (PBA) as host comes from previous studies on different upconverters. This rubber is obtainable under mild reaction conditions with good optical quality,[36] and its local viscoelasticity does not prevent the molecular diffusion, which is mandatory for promoting the ET from sensitizers to *n*MOFs. Taking into account their structure, size and density, we estimate that the concentration of nanocrystals in the sample is ~2×10^{14} cm^{-3} (3.2×10^{-7} M, see SI). This

is the highest concentration that enables to obtain a homogenous bulk material without any macroscopic aggregation of nanocrystals after the polymerization reaction (Fig. S6). On the other side, the loading of rubbers with nano-fillers is well known to potentially affect their mechanical properties. Especially relevant for our purpose it is the interaction between the nanocrystals surface and the polymeric host. In particular, polymer chains can be adsorbed on the surface and create an extended interphase of pronounced rigidity that can reduce the mobility of diffusing sensitizers and also potentially avoid a direct contact.[41, 42] We performed therefore a series of mechanical and structural characterization experiments (Fig. S4) in order to monitor the material viscoelastic properties at the employed loading levels. The analyses demonstrate an intimate mixing of *n*MOFs with the soft host phase, without detrimental consequences on the diffusivity of PtOEPs.

We study the nanocomposite emission properties by means of steady state and time-resolved photoluminescence measurements. As showed in Fig. 3a, under excitation with a continuous wave (CW) doubled Nd:YAG laser at 532 nm, the material shows the peculiar photoluminescence spectrum of a *s*TTA upconversion system where, beside the residual emission of PtOEP due to an incomplete ET (Φ_{ET} = 0.60, Fig. S5), we observe an anti-Stokes emission from *n*MOFs peaked at 440 nm. The inset shows that the blue emission is visible even with naked eyes through a short pass optical filter. The effects of the embedding on nanocrystals are analyzed by monitoring their fluorescence under pulsed excitation at 340 nm. Figure 3b compares the fluorescence decays of *n*MOFs dispersed in benzene and PBA with that one of the ABD ligand in PBA. In benzene, the time resolved PL spectrum of *n*MOFs behaves as a multi-exponential function with an average lifetime of 1.3 ns (see SI), which is about five times shorter than the one of ADB dispersed in PBA (6.1 ns). This decay dynamic is ascribed to a distribution of quenching centers that open additional non-radiative recombination pathways. This implies the drop of QY_{fl} from 85% for ADB in benzene down to 17% for the *n*MOFs

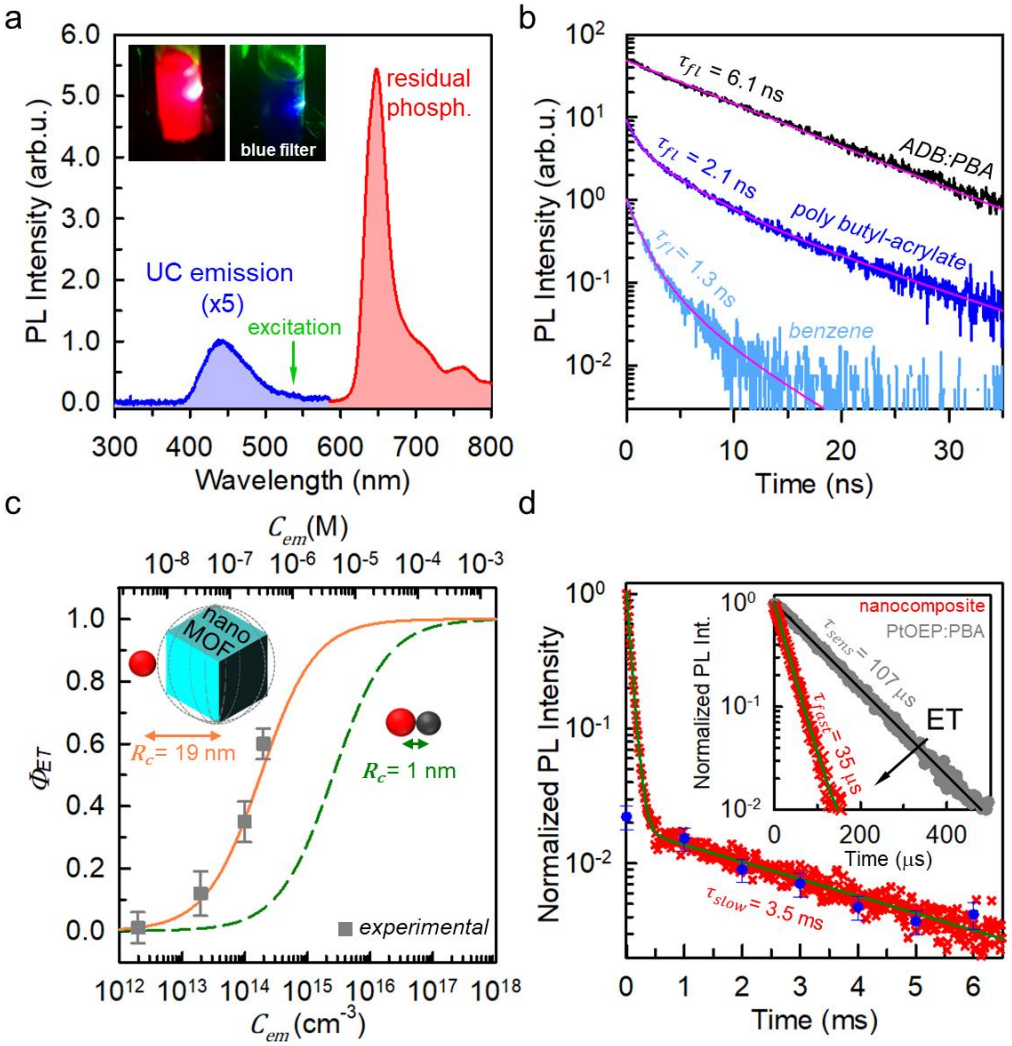

Figure 3. a) Photoluminescence (PL) spectrum of the nanocomposite under CW laser illumination at 532 nm (100 mW cm^{-2}). Inset: Digital pictures of the sample recorded without (left) and with a short pass blue optical filter (right). b) Time-resolved fluorescence spectrum at 435 nm of *n*MOFs dispersed in benzene and in *poly* butyl-acrylate (PBA), compared with the decay of the isolated ligand ADB in PBA dispersion, under pulsed excitation at 340 nm. Solid line are the fit with a multiexponential decay function. c) Calculated and experimental energy transfer yield Φ_{ET} from PtOEP to *n*MOFs as a function of the nanocrystals concentration C_{em}. The theoretical Φ_{ET} is calculated in the Perrin approximation using a sensitizer/emitter contact radius R_c of 1 nm (dashed line) and 19 nm (solid line). d) Time resolved PL spectrum of the nanocomposite at 645 nm (crosses) and 435 nm (dots), under modulated excitation at 532 nm (10 mW cm^{-2}). Inset: comparison of the PL decay at 645 nm between the nanocomposite and a PtOEP-doped PBA sample (PtOEP:PBA).

dispersion. This effect is mitigated by the embedding of nanocrystals in the polymer that partially passivates their surfaces thus reducing the number of quenching centers.[26] Consequently, the average fluorescence lifetime rises to 2.10 ns in the nanocomposite, which corresponds to an increase of QY_{fl} up to ~30%, as confirmed by the 28±4% yield measured with an integrating sphere (Fig. S10). The multi-exponential character of the emission decay

suggests also the absence of significant leaking of ligands from *n*MOFs due to the degradation of the crystalline structure, since isolated ADBs in PBA show different recombination dynamics.

Photoluminescence spectroscopy enables the analysis of the ET step, which requires a special care because it involves a small donor molecule, as the PtOEP, and a supramolecular system as a giant acceptor. The Dexter ET involved is a short-range interaction, which needs the physical collision between two moieties to occur. When small molecules are employed, the contact distance R_c between the donor and the acceptor is usually given by the sum of the molecular radii $R_c = R_d + R_a \approx$ 1-2 nm.[34, 43] The nanocomposite offers a different scenario. Each *n*MOF contains many closely packed acceptors, and only those on the surface are involved in the ET when an excited sensitizer hits the nanocrystal. We describe therefore each *n*MOF as an ideal spherical acceptor of radius R_{nMOF}. This means that R_c increases to a length of tenth of nanometres, thus an efficient transfer can be achieved by using relatively small densities of acceptors. Indeed, even if the nanocomposite contains a low amount of *n*MOFs that usually prevents the Dexter ET in viscous environments such as PBA, we observe a transfer yield larger than 50%.[34, 43] In order to test quantitatively our model, we compare the measured Φ_{ET} as a function of the acceptor/emitter concentration C_{em} (Fig. S6) with the values predicted in the *rapid diffusion limit* for different interaction radii (Fig. S6 and Fig. 3c). In this condition, the transfer rate is proportional to C_{em} and it is calculated as $k_{ET} = 4\pi D_{sens} C_{em} R_c$, where D_{sens} = 9.0×10^{-7} cm^2 s^{-1} is the sensitizer diffusivity in PBA.[17, 20, 38] Due to their size, the diffusivity of nanocrystals is considered negligible. The expected transfer yield is calculated as $\Phi_{ET}(C_{em}) = \frac{k_{ET}(C_{em})}{k_{ET}(C_{em})+k_{sens}}$, where $k_{sens} = (\tau_{sens})^{-1}$ is the spontaneous recombination rate of PtOEP in absence of acceptors.[38] The dashed line in Fig. 3c shows the transfer yield calculated for R_c = 1 nm, which clearly underestimates the observed values (squares). Conversely, the experimental data can be fitted with the theoretical Φ_{ET} function calculated for R_c= 19 nm (solid line). This length is intermediate between the radius of the inscribed and circumscribed sphere to a cube

with edge of 26 nm, i.e. the *n*MOFs average dimension inferred from the TEM data analysis. The diffusion-assisted nature of the ET observed in the nanocomposite is further confirmed by a low temperature experiment. The cooling of the material to 77 K (Fig. S6) leads to the disappearance of the upconverted emission and to the appearance of a strong PtOEP phosphorescence, due to suppression of the ET in the frozen polymer where the sensitizers are blocked and cannot reach the acceptors. Therefore, these findings validate the proposed model for the diffusion-assisted Dexter-type interaction between a small molecule donor and a giant acceptor species.

The time resolved analysis of the sensitizer residual phosphorescence is consistent with the proposed picture and gives us further insights on the PtOEP/*n*MOFs interaction. By exciting the PtOEPs with a modulated CW laser at 532 nm, Fig. 3d shows that the luminescence at 645 nm decays as a single exponential function for about 300 μs, which corresponds to a signal decrease of more than 90%. This behavior confirms that the ET occurs in the rapid diffusion limit.[43] The corresponding decay time τ_{fast} is 35 μs (inset). Notably, the spectrum shows a secondary slow decay component, which accounts for 2% of the total phosphorescence intensity. The lifetime of this component is τ_{slow}= 3.5 ms, which is even longer than the PtOEP radiative decay time in PBA (τ_{sens} = 107 μs).[44] While the fastest component reflects the transfer from PtOEPs to nanocrystals, this slow luminescence is ascribed to a back energy transfer (back-ET) from *n*MOFs to sensitizers. Because the *n*MOF triplet has a lifetime significantly longer than the PtOEP triplet, the re-population from nanocrystals results in an *apparent* extra-long living delayed phosphorescence, which mirrors the spontaneous lifetime of nanocrystals triplets. Importantly, the presence of back-ET implies that the ET yield obtained from time resolved data, $\Phi_{ET}^{'} = \left(1 - \tau_{fast}/\tau_{sens}\right) \sim 0.70$ overestimates the net transfer yield measured in steady state conditions Φ_{ET} = 0.60 (Fig. S5).[13, 45] The occurrence of back-ET is not usually detected in molecular system based on PtOEP and polyacenes at the employed concentrations, which

suggests that it arises from the peculiar nature of our emitters for confined-TTA, as discussed in the next section.

The peculiar behaviour of *s*TTA upconversion in MOF-based nanocomposites it is studied by a side-by-side comparison with respect to a standard bi-component organic solution, i.e. a mixture of DPA (10^{-2} M) and PtOEP (10^{-4} M) in tetrahydrofuran. Fig. 4b shows the log-log plot of the photon upconversion efficiency of the nanocomposite (triangles) and of the reference (dots) measured as a function of the excitation intensity I_{exc} at 532 nm in steady state condition on oxygen free samples (see Methods). The reference shows the typical behaviour of bulk systems where triplet excitons are free to move in an infinite volume. Until saturation at high powers, the upconversion yield rises smoothly with the excitation intensity, due to the increment of the triplets population that boosts the annihilation rate k_{TTA} in respect to the spontaneous recombination k_T. This behaviour is described by

$$\mathrm{QY_{uc}}(I_{exc}) = \frac{1}{2} f\ \mathrm{QY_{fl}} \Phi_{ET} \Phi_{TTA}(I_{exc}) = \frac{1}{2} f\ \mathrm{QY_{fl}} \Phi_{ET} \left[\frac{k_{TTA}(I_{exc})}{k_{TTA}(I_{exc}) + k_T}\right], \qquad \text{Eq. 1}$$

where f = 0.5, $\mathrm{QY_{fl}}$ = 0.96 and Φ_{ET} = 1 for the considered solution (dashed line). [13] The yield Φ_{TTA} is the only power dependent parameter, calculated by considering the dyes diffusivities.[21]

The nanocomposite behaves differently, with a sharper transition from the low efficiency regime to the saturation that derives from the different annihilation dynamic in a confined environment where $L_T \gg d$. As sketched in Fig. 4b, when two excitons coexist in a *n*MOF they annihilates producing a fluorescent singlet, thus giving rise to a *UC-bright* nanocrystal with $\Phi_{TTA} = 1$ that is a thresholdless annihilator. Conversely, if only one exciton is present, the nanocrystal remains *UC-dark*. In this case, the triplet dissipates its energy by back-ET or spontaneous recombination. The overall performance of the nanocomposite must be described therefore by considering the statistical distribution of the exciton population in the nanocrystal ensemble as function of the excitation intensity, instead of in term of the power- and diffusion-dependent annihilation rates.

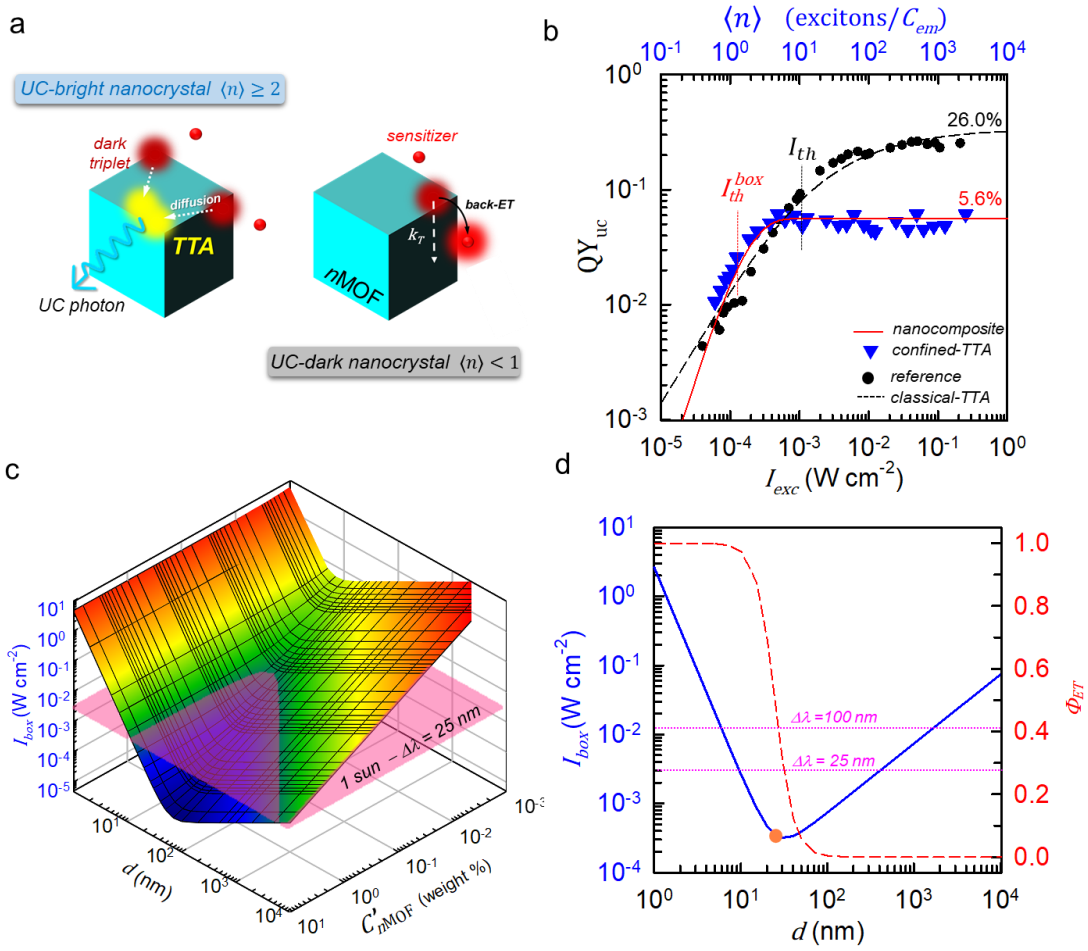

Figure 4. a) Sketch of the recombination dynamics of triplet excitons in UC-dark and UC-bright MOF nanocrystals. If the average number of triplets created in a single nanocrystal is $\langle n \rangle \geq 2$, TTA can occur with 100% yield and thus we have a *UC-bright* *n*MOFs. Conversely, if $\langle n \rangle < 2$, the nanocrystal is *UC-dark*, because the isolated triplet can only recombine spontaneously with a rate k_T or back transfer (back-ET) its energy to a sensitizer that hits the crystal surface. b) Comparison of the upconversion quantum yield (QY_{uc}) measured as a function of the excitation intensity I_{exc} for the *s*TTA-UC nanocomposite (triangles) and for a standard DPA/PtOEP (10^{-2} M:10^{-4} M) solution in tetrahydrofuran (dots). The conversion efficiency for the nanocomposite is reported also as a function of the average number of exciton per nanocrystal $\langle n \rangle$ calculated for each I_{exc}. Dashed and solid line are the theoretical QY_{uc} predicted respectively for the classical reference solution (classical-TTA) and of the threshold less up-converting nanocrystals (confined-TTA), as described in the text. c) Calculation of the threshold I_{th}^{box} as a function of the *n*MOFs density (C_{em}) and of the nanocrystal size *d*. The pink plane indicated AM1.5 solar irradiance at 532 nm with a bandwidth of $\Delta\lambda$=25 nm. d) Plot of the I_{th}^{box} and energy transfer yield Φ_{ET} as function of the *n*MOFs size *d* calculated for the C_{em} used in the nanocomposite. Dotted lines indicate the AM1.5 solar irradiance at 532 nm with different bandwidths. The orange dot marks the observed threshold for the nanocomposite used in our experiments.

In this case, the conversion yield is

$$\mathrm{QY_{uc}} = \frac{1}{2} f \, \mathrm{QY_{fl}} \Phi_{ET} P_{n\geq 2}(I_{exc}). \qquad \text{Eq. 2}$$

where P_n is the cumulative probability to have at least *n* excitons in the same *n*MOF in absence of annihilation. This latter can be calculated by means of the Poisson distribution function.

$P_{n\geq 2}$ quantifies the fraction of *UC-bright* nanocrystals, i.e. the upconversion active population, and depends only on I_{exc}, which determines the centre of the poissonian distribution of excitons per nanocrystal $\langle n \rangle$. As showed in Fig. 4b, the model reproduces accurately the experimental data. The solid line is the plot of QY_{uc} vs. I_{exc} calculated by Eq. 2 using f = 0.5[13] and experimentally determined power independent quantities. Data in Fig. 4a show a QY_{uc}^{max} of ~6%, in very good agreement with the maximum yield of ~5 % predicted by Eq. 2 considering $P_{n\geq 2}$ =1 and the experimental Φ_{ET} = 0.60 and QY_{fl} = 0.28 values.[13] Notably, these latter efficiencies are the parameters that actually limit the overall upconversion performance, which can be raised up by improving the *n*MOFs surface passivation and employing different polymeric host in order to reach the theoretical maximum upconversion yield.

It is worth pointing out that the calculation of $\langle n \rangle$ does require to know the ratio between the excitation rate and the recombination rate k_T of confined triplets (see SI). However, the instantaneous occurrence of TTA in UC-bright *n*MOFs prevents obtaining k_T from the long-time tail of standard time-resolved photoluminescence measurements (Fig. 1b).[46] In order to bypass this problem, we set up a pump and probe experiment in which the sample is first excited with a strong light pulse and then is probed with additional weak and short pulses at different delays Δt (Fig. S7).[47] The first pulse generates the upconverted emission, after which only triplets in UC-dark nanocrystals survives. The probe pulses, by generating few additional triplet, make bright few of the dark *n*MOFs without altering significantly the number of excitons. In such a way, by monitoring the upconverted emission intensity synchronized with the probe pulses, we follow the time evolution of the triplets population in UC-dark nanocrystals obtaining k_T= 286 Hz, a value similar to that one of anthracene-like emitters in organic solvents thank to the surface-defect passivation by the polymer.[48] Notably, the observed triplet decay matches the slow component of the sensitizer residual phosphorescence (Fig. 3d), which confirms that this latter is due to back-ET from UC-dark *n*MOFs.[46]

The results obtained show that the key advantage of the nanocomposite is that it reaches the maximum upconversion efficiency at excitation intensity lower than the solution. We quantify this performance improvement by monitoring the turn on of the high-efficiency regime that is marked by I_{th}. In bulk-TTA, I_{th} is defined as the excitation intensity at which k_{TTA} equals k_T, but this definition is not more applicable for *n*MOFs, where annihilation is the only effective decay pathway for confined triplet pairs. However, according to Eq.1, I_{th} corresponds also to the excitation condition at which the system shows a conversion yield of 50% of its maximum value. Likewise, we define the critical excitation intensity I_{th}^{box} for confined-TTA as the irradiance at which $\mathrm{QY_{uc}}\left(I_{th}^{box}\right) = 0.5\mathrm{QY_{uc}^{max}}$. According to Eq. 2, this happens when I_{th}^{box} gives $P_{n\geq 2}$= 0.5, i.e. when 50% of the nanocrystals in the ensemble contains at least two triplets. This condition is satisfied when is $\langle n\rangle = 1.7$. Consequently, taking into account the absorption coefficient α [cm^{-1}], Φ_{ET}, the nanocrystal concentration C_{em} and the spontaneous decay rate of *n*MOF triplets, the analytical definition of the excitation threshold in confined-TTA systems results as (see SI)

$$I_{th}^{box} = \langle n\rangle_{P_{n\geq 2}} \frac{k_T C_{em}}{\alpha \Phi_{ET}} = 1.7 \frac{k_T C_{em}}{\alpha \Phi_{ET}} . \qquad \text{Eq. 3}$$

The predicted I_{th}^{box} for our material is ~2×10^{-4} W cm^{-2}, which is in very good agreement with the experimental data and, remarkably, it is one order of magnitude lower than the threshold I_{th} ~1.6×10^{-3} W cm^{-2} of the reference solution. I_{th}^{box} corresponds to an incident photon flux of 5.4×10^{14} ph cm^{-2} s^{-1} at 532 nm, which is twenty times smaller than the AM1.5 solar irradiance in the low-energy absorption band of the PtOEP.[49] It follows that the nanocomposite reaches $\mathrm{QY_{uc}^{max}}$ under few percent of the sun irradiance, thus overmatching the requirement of solar technologies.

Eq. 3 point out the factors that rule the upconversion efficiency and therefore it can be used to understand where there is room for improvements. First, I_{th}^{box} depends linearly on the

spontaneous decay rate of the triplets, which is strongly affected by the presence of quenching centres. Therefore, improved synthesis protocols that produce defect-free nanocrystals will allow reducing the threshold by decreasing k_T. The same result can be obtained by extending the absorption bandwidth of the sensitizer to increase the fraction of harvested solar photons. In this case, the absorption coefficient α must be replaced with the bandwidth-integrated absorptance $\alpha' = \int \alpha(\lambda) d\lambda$. The last two parameters to discuss are the transfer yield Φ_{ET} and the nanocrystals concentration C_{em}, which are strictly related each other because the transfer rate is proportional to C_{em}. In particular, a reduction of C_{em} would in principle lower the threshold by increasing $\langle n \rangle$. However, the same reduction will result in a decrease of Φ_{ET} that will affect the threshold in the opposite way. Therefore, a trade-off between these two effects must be found. Fig. 4c reports the calculated as function of the *n*MOFs size d and the weight concentration C'_{em} of embedded nanocrystals. The nanocrystals size ranges from one nm, i.e. the molecular case, to 10^4 nm, while C'_{em} is varied between 0.01% and 10%. The calculation demonstrates that the threshold decreases by increasing the amount of nanocrystals, which enhances the ET rate and efficiency. The minimum threshold, corresponding to the optimal trade-off between Φ_{ET} and $\langle n \rangle$, is found as low as 3×10^{-6} W cm^{-2} for a C'_{em} = 10% and nanocrystals of size d = 200 nm. Importantly, this threshold corresponds to ~10^{-3} suns considering the sensitizer absorption at 532 nm with a bandwidth of $\Delta\lambda$=25 nm. In our case, the maximum loading level that allows having and homogeneous samples is C'_{em}= 0.33%. Fig. 4d shows the I_{th}^{box} calculated as function of d for this concentration. The minimum value of 3×10^{-4} W cm^{-2} is predicted for d = 32 nm, very close to the size of the employed nanocrystals, which is equivalent to an irradiance of 0.06 suns. Interestingly, the corresponding Φ_{ET} is relatively low, about 25%. The transfer yield (dashed line) quickly saturates to 100% using smaller nanocrystals with d < 10 nm, because of the increased number of acceptors, but the simultaneous reduction of $\langle n \rangle$ pushes I_{th}^{box} to super-solar values. Conversely, Φ_{ET} becomes the

factor limiting the system performances for d > 70 nm, because the number of *n*MOFs is so low that the ET is almost prevented.

This analysis highlights that tailoring the dimension of nanosized annihilators is of outmost importance for the realization of an efficient composite upconverter. However, it is also important to outline that Eq. 3 gives a subsolar threshold using nanocrystals with size between 20 nm and 60 nm (Fig. 4d). This is pivotal for the material development, because this finding mitigates a potential strict constraint that would require an extremely careful control of the synthesis route to achieve monodispersed sizes. This advantage will be further enhanced using nanocomposites with extended absorption bandwidths. Indeed, with a $\Delta\lambda$=100 nm the threshold will be about few percent of one sun even using nanocrystals with sizes ranging from 10 to 300 nm. Therefore, exploiting this relaxed condition, more efforts can be focused on to the preparation of high quality and defect-free nanocrystals as improved annihilators/emitters. Importantly, the findings presented are related to the structural properties of nanocrystals. In particular, the density of the acceptor/emitter moiety in the framework plays a fundamental role. For example, using *n*MOF with ADB ligands packed in closer configuration would be more favorable to the creation of coupled triplet pairs, by enhancing both the ET and the exciton diffusivity. Another interesting approach has been recently explored by Rowe and co-workers, which obtained upconversion in MOF functionalized with surface-bound sensitizers. This configuration assure a 100% ET yield without any molecular diffusion, but the low conversion yields reported suggest that further studies are required to shed light on the role of the surface sensitizer in both back-ET and MOF fluorescence mechanisms.[28] Moreover, for solar applications this design implies that the amount of light harvesters per MOF is limited by the functionalization reaction yield with consequences on the optical density of the bulk composite that must be evaluated.

In conclusion, we demonstrated that the confinement of triplet pairs in MOF nanocrystals with sizes of tenths of nanometers, i.e. smaller than the diffusion length of triplet excitons, makes the probability of spontaneous recombination negligible in respect to the bimolecular annihilation rate, thus achieving thresholdless upconverters with a triplet annihilation yield of 100%. Even if the corresponding nanocrystal ensemble shows a threshold excitation intensity for achieving the maximum conversion yield, which depends on the statistical distribution of the excitation energy among the upconverting units, I_{th}^{box} is well below the solar irradiance. The performance of this system has been modelled and a simple expression for I_{th}^{box} has been obtained. The proposed model has been validated by using multicomponent nanocomposites, which consists of a rubber polymer matrix doped with triplet sensitizer dyes and loaded with annihilating/emitting MOF nanocrystals. Our system, thanks to a proper surface-defect passivation and to the optimized sensitizer and MOF concentrations, shows a threshold of few percent of the solar irradiance, which is one order of magnitude lower than the best solution-based systems developed in the last decade. Therefore, while more efforts must be focused in the development of highly emissive MOF nanocrystals, this nanocomposites represent the first prototype of the next generation of low power photon upconverters potentially suitable for real world solar applications.

ASSOCIATED CONTENT

Supporting Information.

Experimental methods, additional data and figures that support the structural and optical characterization of the MOF nanocrystals and nanocomposites, together with the details on the time resolved photoluminescence spectroscopy measurements performed and the exciton distribution calculation.

AUTHOR INFORMATION

Corresponding Authors

* Email: angelo.monguzzi@unimib.it

Author Contributions

The manuscript was written through contributions of all authors. All authors have given approval to the final version of the manuscript.

Notes

The authors declare no competing financial interest.

ACKNOWLEDGMENT

A.M. acknowledges support from Università degli Studi Milano-Bicocca (Grant No. 2016 ATESP0052) and the Cariplo Foundation (Grant No. 2016-0925).

REFERENCES

1. Congreve, D. N.; Lee, J.; Thompson, N. J.; Hontz, E.; Yost, S. R.; Reusswig, P. D.; Bahlke, M. E.; Reineke, S.; Van Voorhis, T.; Baldo, M. A. *Science* **2013,** 340, (6130), 334-7.
2. Rao, A.; Friend, R. H. *Nature Reviews Materials* **2017,** 2, 17063.
3. Uoyama, H.; Goushi, K.; Shizu, K.; Nomura, H.; Adachi, C. *Nature* **2012,** 492, (7428), 234-8.
4. Nakanotani, H.; Higuchi, T.; Furukawa, T.; Masui, K.; Morimoto, K.; Numata, M.; Tanaka, H.; Sagara, Y.; Yasuda, T.; Adachi, C. *Nature Communications* **2014,** 5, 4016.
5. Monguzzi, A.; Borisov, S. M.; Pedrini, J.; Klimant, I.; Salvalaggio, M.; Biagini, P.; Melchiorre, F.; Lelii, C.; Meinardi, F. *Advanced Functional Materials* **2015,** 25, (35), 5617-5624.
6. Li, C.; Koenigsmann, C.; Deng, F.; Hagstrom, A.; Schmuttenmaer, C. A.; Kim, J.-H. *ACS Photonics* **2016,** 3, (5), 784-790.
7. Kim, H.-i.; Kwon, O. S.; Kim, S.; Choi, W.; Kim, J.-H. *Energy & Environmental Science* **2016,** 9, (3), 1063-1073.
8. Wu, M.; Congreve, D. N.; Wilson, M. W. B.; Jean, J.; Geva, N.; Welborn, M.; Van Voorhis, T.; Bulović, V.; Bawendi, M. G.; Baldo, M. A. *Nature Photonics* **2015,** 10, 31.
9. Vadrucci, R.; Monguzzi, A.; Saenz, F.; Wilts, B. D.; Simon, Y. C.; Weder, C. *Advanced Materials* **2017,** 29, (41), 1702992.
10. Hill, S. P.; Dilbeck, T.; Baduell, E.; Hanson, K. *ACS Energy Letters* **2016,** 1, (1), 3-8.
11. Baluschev, S.; Miteva, T.; Yakutkin, V.; Nelles, G.; Yasuda, A.; Wegner, G. *Physical Review Letters* **2006,** 97, (14), 143903.
12. Singh-Rachford, T. N.; Castellano, F. N. *Coordination Chemistry Reviews* **2010,** 254, (21), 2560-2573.
13. Monguzzi, A.; Tubino, R.; Hoseinkhani, S.; Campione, M.; Meinardi, F. *Physical Chemistry Chemical Physics* **2012,** 14, (13), 4322-4332.
14. Schulze, T. F.; Schmidt, T. W. *Energy & Environmental Science* **2015,** 8, (1), 103-125.
15. Gray, V.; Moth-Poulsen, K.; Albinsson, B.; Abrahamsson, M. *Coordination Chemistry Reviews* **2018,** 362, 54-71.
16. Hoseinkhani, S.; Tubino, R.; Meinardi, F.; Monguzzi, A. *Physical Chemistry Chemical Physics* **2015,** 17, (6), 4020-4024.
17. Inokuti, M.; Hirayama, F. *The Journal of Chemical Physics* **1965,** 43, (6), 1978-1989.
18. Parker, C. A., *Photoluminescence of solutions : With applications to photochemistry and analytical chemistry*. Elsevier: Amsterdam, London, N.Y., 1968.
19. Jortner, J.; Choi, S.-i.; Katz, J. L.; Rice, S. A. *Physical Review Letters* **1963,** 11, (7), 323-326.
20. Gösele, U.; Hauser, M.; Klein, U. K. A.; Frey, R. *Chemical Physics Letters* **1975,** 34, (3), 519-522.
21. Monguzzi, A.; Mezyk, J.; Scotognella, F.; Tubino, R.; Meinardi, F. *Physical Review B* **2008,** 78, (19), 195112.
22. Dilbeck, T.; Hill, S. P.; Hanson, K. *Journal of Materials Chemistry A* **2017**.
23. Cheng, Y. Y.; Fückel, B.; Khoury, T.; Clady, R. G. C. R.; Tayebjee, M. J. Y.; Ekins-Daukes, N. J.; Crossley, M. J.; Schmidt, T. W. *The Journal of Physical Chemistry Letters* **2010,** 1, (12), 1795-1799.
24. Yanai, N.; Kimizuka, N. *Accounts of Chemical Research* **2017,** 50, (10), 2487-2495.
25. Zhou, H.-C.; Long, J. R.; Yaghi, O. M. *Chemical Reviews* **2012,** 112, (2), 673-674.
26. Monguzzi, A.; Ballabio, M.; Yanai, N.; Kimizuka, N.; Fazzi, D.; Campione, M.; Meinardi, F. *Nano Letters* **2018,** 18, (1), 528-534.

27. Park, J.; Xu, M.; Li, F.; Zhou, H.-C. *Journal of the American Chemical Society* **2018,** 140, (16), 5493-5499.
28. Rowe, J. M.; Zhu, J.; Soderstrom, E. M.; Xu, W.; Yakovenko, A.; Morris, A. J. *Chemical Communications* **2018,** 54, (56), 7798-7801.
29. Ern, V. *The Journal of Chemical Physics* **1972,** 56, (12), 6259-6260.
30. Najafov, H.; Lee, B.; Zhou, Q.; Feldman, L. C.; Podzorov, V. *Nature Materials* **2010,** 9, 938.
31. Grisanti, L.; Olivier, Y.; Wang, L.; Athanasopoulos, S.; Cornil, J.; Beljonne, D. *Physical Review B* **2013,** 88, (3), 035450.
32. Sternlicht, H.; Nieman, G. C.; Robinson, G. W. *The Journal of Chemical Physics* **1963,** 38, (6), 1326-1335.
33. Bachilo, S. M.; Weisman, R. B. *The Journal of Physical Chemistry A* **2000,** 104, (33), 7711-7714.
34. Stryer, L.; Thomas, D. D.; Meares, C. F. *Annual Review of Biophysics and Bioengineering* **1982,** 11, (1), 203-222.
35. Singh-Rachford, T. N.; Lott, J.; Weder, C.; Castellano, F. N. *Journal of the American Chemical Society* **2009,** 131, (33), 12007-12014.
36. Monguzzi, A.; Mauri, M.; Bianchi, A.; Dibbanti, M. K.; Simonutti, R.; Meinardi, F. *The Journal of Physical Chemistry C* **2016,** 120, (5), 2609-2614.
37. Scholes, G. D. *Annual Review of Physical Chemistry* **2003,** 54, (1), 57-87.
38. Monguzzi, A.; Tubino, R.; Salamone, M. M.; Meinardi, F. *Physical Review B* **2010,** 82, (12), 125113.
39. Mattiello, S.; Monguzzi, A.; Pedrini, J.; Sassi, M.; Villa, C.; Torrente, Y.; Marotta, R.; Meinardi, F.; Beverina, L. *Advanced Functional Materials* **2016,** 26, (46), 8447-8454.
40. Hiemenz, P. C.; Lodge, T., *Polymer chemistry*. CRC Press: Boca Raton, 2007.
41. Sharma, S. K.; Sudarshan, K.; Pujari, P. K. *Physical Chemistry Chemical Physics* **2016,** 18, (36), 25434-25442.
42. Tadiello, L.; D'Arienzo, M.; Di Credico, B.; Hanel, T.; Matejka, L.; Mauri, M.; Morazzoni, F.; Simonutti, R.; Spirkova, M.; Scotti, R. *Soft Matter* **2015,** 11, (20), 4022-4033.
43. Thomas, D. D.; Carlsen, W. F.; Stryer, L. *Proceedings of the National Academy of Sciences of the United States of America* **1978,** 75, (12), 5746-5750.
44. Bansal, A. K.; Holzer, W.; Penzkofer, A.; Tsuboi, T. *Chemical Physics* **2006,** 330, (1), 118-129.
45. Lakowicz, J. R., *Principles of fluorescence spectroscopy*. Springer: New York, 2010.
46. Pope, M.; Swenberg, C. E. *Annu. Rev. Phys. Chem. Annual Review of Physical Chemistry* **1984,** 35, (1), 613-655.
47. Monguzzi, A.; Mauri, M.; Frigoli, M.; Pedrini, J.; Simonutti, R.; Larpent, C.; Vaccaro, G.; Sassi, M.; Meinardi, F. *The Journal of Physical Chemistry Letters* **2016,** 7, (14), 2779-2785.
48. Montalti, M.; Murov, S. L., *Handbook of photochemistry*. Taylor & Francis: Boca Raton, Fla., 2006.
49. Monguzzi, A.; Oertel, A.; Braga, D.; Riedinger, A.; Kim, D. K.; Knüsel, P. N.; Bianchi, A.; Mauri, M.; Simonutti, R.; Norris, D. J.; Meinardi, F. *ACS Applied Materials & Interfaces* **2017,** 9, (46), 40180-40186.

TOC

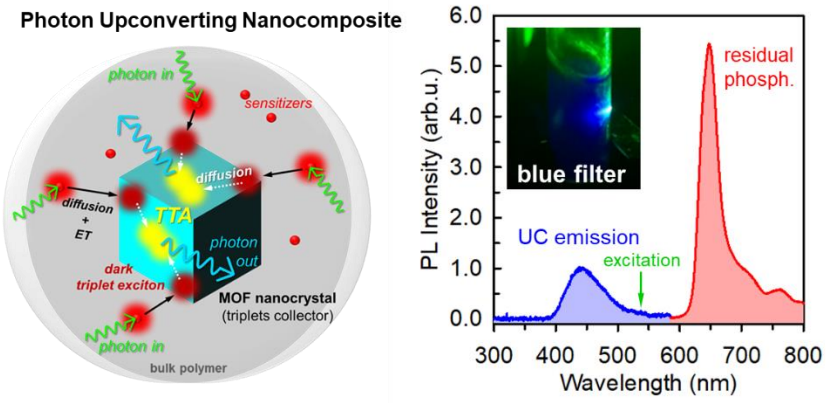
Photon Upconverting Nanocomposite
photon in
sensitizers
diffusion
diffusion
+
ET
TTA
photon
out
dark
triplet exciton
MOF nanocrystal
(triplets collector)
photon in
bulk polymer
blue filter
residual
phosph.
UC emission
excitation
PL Intensity (arb.u.)
Wavelength (nm)
6.0
5.0
4.0
3.0
2.0
1.0
0.0
300
400
500
600
700
800